

# Description of Four-Body Breakup Reaction with the Method of Continuum-Discretized Coupled-Channels

Tomoaki EGAMI,<sup>1</sup> Takuma MATSUMOTO,<sup>2</sup> Kazuyuki OGATA<sup>1</sup> and Masanobu YAHIRO<sup>1</sup>

<sup>1</sup>*Department of Physics, Kyushu University, Fukuoka 812-8581, Japan*

<sup>2</sup>*RIKEN Nishina Center, Wako 351-0198, Japan*

We present a method of smoothing discrete breakup  $S$ -matrix elements calculated by the method of continuum-discretized coupled-channels (CDCC). This smoothing method makes it possible to apply CDCC to four-body breakup reactions. The reliability of the smoothing method is confirmed for two cases,  $^{58}\text{Ni}(d, pn)$  at 80 MeV and the E1 transition of  $^6\text{He}$ . We apply CDCC with the smoothing method to a  $^6\text{He}$  breakup reaction at 22.5 MeV. Multistep breakup processes are found to be important.

## §1. Introduction

Recent developments in radioactive beam experiments have made it possible to study unstable nuclei away from the stability line. Such nuclei have exotic properties, e.g., the halo structure,<sup>1)-3)</sup> in which weakly bound valence neutrons extend far from a core nucleus. Borromean nuclei such as  $^6\text{He}$  and  $^{11}\text{Li}$  are typical examples of halo nuclei and are described well by a three-body ( $n+n+\text{core}$ ) model. In the scattering of a three-body projectile, it easily breaks up into its constituents, and hence the reaction should be described as four-body ( $n+n+\text{core}+\text{target}$ ) scattering.

Thus far, many experiments have been conducted on the scattering of  $^6\text{He}$  from heavy<sup>4)-10)</sup> to light targets<sup>9)-12)</sup> at high<sup>8)-11)</sup> and low incident energies.<sup>4)-7), 12)</sup> From the theoretical point of view, it is quite difficult to solve four-body scattering exactly. At higher incident energies, therefore, the scattering has been analyzed using approximate methods such as the Glauber model,<sup>13), 14)</sup> adiabatic approximation,<sup>15), 16)</sup> multiple scattering expansion<sup>17)</sup> and the four-body DWBA.<sup>18)-20)</sup> These methods are, however, not applicable to scattering at low incident energies.

One of the most useful and reliable methods for the scattering in a wide range of incident energies is the method of continuum-discretized coupled channels (CDCC).<sup>21), 22)</sup> In CDCC, the total scattering wave function is expanded in terms of the complete set of bound and continuum states of the projectile. The continuum states are classified by linear and angular momenta,  $k$  and  $\ell$ , respectively; each of them is truncated at a certain value. The  $k$ -continuum is then divided into small bins and the continuum states in each bin are averaged into a single state. This procedure of discretization is called the average method. The  $S$ -matrix elements calculated with CDCC converge as the model space is extended.<sup>23), 24)</sup> The converged CDCC solution is the unperturbed solution of the distorted Faddeev equations, and corrections to the solution are negligible within the region of space in which the reaction takes place.<sup>25), 26)</sup>

Conventional CDCC based on the average method has been applied only to three-body breakup processes in the scattering of two-body projectiles. It is thus

called *three-body CDCC*. For four-body breakup processes in the scattering of three-body projectiles, the average method is not feasible, since it requires exact three-body continuum states of the projectile that are quite difficult to obtain. This problem can be circumvented by the pseudostate discretization method instead of the average method. In the pseudostate discretization method, the continuum states are replaced with pseudostates obtained by diagonalizing the internal Hamiltonian of the projectile in a space spanned by  $L^2$ -type basis functions. One can adopt the Gaussian<sup>27),28)</sup> or transformed harmonic oscillator (THO)<sup>29)</sup> basis as the  $L^2$ -type basis functions. The validity of the pseudostate discretization method was confirmed in the scattering of two-body projectile by the good agreement between the CDCC solutions obtained by the pseudostate discretization and the average methods.

The pseudostate discretization method makes CDCC applicable to the scattering of three-body projectiles. In fact, *four-body CDCC* based on the pseudostate discretization method with Gaussian<sup>30)-32)</sup> or THO<sup>33)</sup> basis functions has been successful in describing the elastic scattering of a three-body projectile at not only high energies but also low energies near the Coulomb barrier. This shows that the back-coupling effects of four-body breakup channels on the elastic scattering, i.e., *virtual* four-body breakup processes, are described well by four-body CDCC. Further development is, however, necessary to apply four-body CDCC to *real* four-body breakup processes, as shown below.

Let us consider the four-body reaction system shown in Fig. 1. The three-body projectile B, which consists of a, b, and c, is incident on the target nucleus A. In the final stage of the breakup reaction considered, four particles, a, b, c, and A, are emitted. The cross section of the reaction is described by the quintuple differential cross section

$$\frac{d^5\sigma}{d\varepsilon_a d\varepsilon_b d\Omega_a d\Omega_b d\Omega_c} \propto |S(\mathbf{k}, \mathbf{K}, \mathbf{P})|^2, \quad (1.1)$$

where  $\varepsilon_a$  ( $\varepsilon_b$ ) is the energy of the emitted particle a (b), and  $\Omega_a$ ,  $\Omega_b$ , and  $\Omega_c$  are the scattering angles of a, b, and c, respectively. This cross section is calculated using the *true* breakup  $S$ -matrix elements  $S(\mathbf{k}, \mathbf{K}, \mathbf{P})$  for the transition of B from the ground states to the continuum states classified with three momenta;  $\mathbf{k}$ ,  $\mathbf{K}$ , and  $\mathbf{P}$  are, respectively, conjugate to the coordinates  $\mathbf{r}$ ,  $\mathbf{y}$ , and  $\mathbf{R}$  shown in Fig. 1. The single differential cross section  $d\sigma/d\varepsilon$  with respect to the intrinsic energy  $\varepsilon$  of B is obtained by integrating Eq. (1.1) over the five variables  $\varepsilon_a$ ,  $\varepsilon_b$ ,  $\Omega_a$ ,  $\Omega_b$ , and  $\Omega_c$  with energy and momentum conservations. However, the breakup  $S$ -matrix elements  $\hat{S}$  calculated using CDCC are discrete functions of  $\varepsilon$ , because of pseudostate discretization, i.e., the diagonalization of the internal Hamiltonian of the projectile. Thus, we need a smoothing method for deriving continuous breakup  $S$ -matrix elements  $S(\mathbf{k}, \mathbf{K}, \mathbf{P})$  from  $\hat{S}$ .

In this paper, we propose a new smoothing method for constructing  $S(\mathbf{k}, \mathbf{K}, \mathbf{P})$  from  $\hat{S}$  to complete four-body CDCC. First, we test the smoothing method in breakup reactions of a two-body projectile and confirm that the breakup  $S$ -matrix elements calculated by the smoothing method agree with the “exact” ones, i.e., the results with the average method of discretization. Next, we apply the smoothing

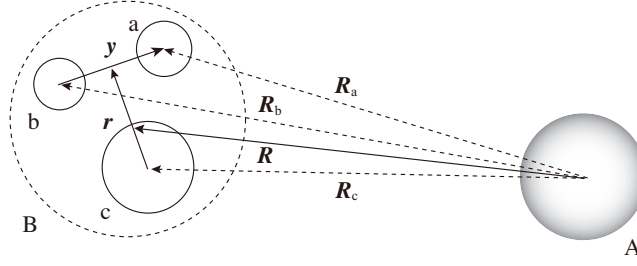


Fig. 1. Illustration of the four-body system; A is the target and B is the projectile composed of the constituents a, b, and c.

method to the electric dipole (E1) transition of  ${}^6\text{He}$  to its continuum states and confirm that the calculated E1 transition strength, with an additional smearing procedure concerning the experimental resolution, converges as the model space is extended. Finally, we apply the smoothing method to four-body breakup reactions of  ${}^6\text{He}$  by  ${}^{209}\text{Bi}$  at 22.5 MeV and show that multistep breakup processes are significant.

This paper is constructed as follows. In §2, we recapitulate four-body CDCC and present a new smoothing method. Test calculations of the smoothing method are shown in §3 and its application to the  ${}^6\text{He}+{}^{209}\text{Bi}$  scattering at 22.5 MeV is shown in §4. Section 5 gives the summary.

## §2. Formulation

### 2.1. Four-body CDCC

We start with the four-body Hamiltonian of the four-body system shown in Fig. 1:

$$H = T_R + U + H_B, \quad (2.1)$$

$$U = U_a(\mathbf{R}_a) + V_a^{\text{Coul}}(\mathbf{R}_a) + U_b(\mathbf{R}_b) + V_b^{\text{Coul}}(\mathbf{R}_b) + U_c(\mathbf{R}_c) + V_c^{\text{Coul}}(\mathbf{R}_c), \quad (2.2)$$

$$H_B = T_r + T_y + V_{bc} + V_{ca} + V_{ab}, \quad (2.3)$$

where  $\mathbf{R}$  is the relative coordinate between the center of masses (cm) of B and A; we assume A to be a structureless and inert nucleus. Note that back-coupling effects of inelastic channels concerning the excitation of A are taken into account with the use of the optical potential between A and each constituent of the projectile, as will be mentioned later. The coordinate  $\mathbf{R}_x$  ( $x = a, b,$  and  $c$ ) denotes the relative coordinate between  $x$  and A, and  $T_\xi$  ( $\xi = \mathbf{R}, \mathbf{r},$  and  $\mathbf{y}$ ) is the kinetic-energy operator associated with  $\xi$ . The interaction  $V_{xx'}$  is the potential between  $x$  and  $x'$ , and  $U_x$  is the optical potential between  $x$  and A; the Coulomb part  $V_x^{\text{Coul}}$  is also accurately treated in order to describe Coulomb breakup processes.

The basic assumption of four-body CDCC is that the four-body reaction takes place in the model space<sup>31), 32)</sup>

$$\mathcal{P} = \sum_i |\hat{\Phi}_i\rangle\langle\hat{\Phi}_i|, \quad (2.4)$$

where  $i$  denotes a set of quantum numbers, i.e., the energy index of the pseudostates  $n$ , the total spin of the projectile  $I$ , and its projection on the  $z$ -axis  $m$ . The pseudostate  $\hat{\Phi}_i (\equiv \hat{\Phi}_{nIm})$  satisfies

$$\langle \hat{\Phi}_i | H_B | \hat{\Phi}_{i'} \rangle = \delta_{ii'} \hat{\varepsilon}_i, \quad (2.5)$$

where  $\hat{\varepsilon}_i$  is the eigenenergy of  $\hat{\Phi}_i$ . The validity of this assumption is justified by the fact that the calculated elastic and total breakup cross sections of the four-body scattering converge as the model space is extended.<sup>27),28),30)–32)</sup> One may thus regard  $\{\hat{\Phi}_i\}$  as a complete set in describing the reaction process considered. We henceforth call  $\{\hat{\Phi}_i\}$  the approximate complete set in this meaning.

Following the discussion above, four-body CDCC starts with the four-body Schrödinger equation in the model space  $\mathcal{P}$ :

$$\mathcal{P}[H - E_{\text{tot}}]\mathcal{P}|\Psi^{\text{CDCC}}\rangle = 0, \quad (2.6)$$

where  $E_{\text{tot}}$  is the total energy of the system. The four-body wave function  $\Psi^{\text{CDCC}}$  is expanded by the approximate complete set  $\{\hat{\Phi}_i\}$ :

$$|\Psi^{\text{CDCC}}\rangle = \sum_i |\hat{\Phi}_i, \hat{\chi}_i\rangle, \quad (2.7)$$

where  $|\hat{\Phi}_i, \hat{\chi}_i\rangle = |\hat{\Phi}_i\rangle \otimes |\hat{\chi}_i\rangle$ , and  $i = 0$  denotes the elastic channel and others ( $i \neq 0$ ) the breakup channels. The expansion coefficient  $|\hat{\chi}_i\rangle$  describes the relative motion between B (in state  $\hat{\Phi}_i$ ) and A. The intrinsic energy  $\hat{\varepsilon}_i$  of B and the relative momentum  $\hat{P}_i$  between B and A satisfy the energy conservation

$$E_{\text{tot}} = E_{\text{in}}^{\text{cm}} + \hat{\varepsilon}_0 = \frac{\hbar^2}{2\mu} \hat{P}_i^2 + \hat{\varepsilon}_i, \quad (2.8)$$

where  $\mu$  is the reduced mass between B and A, and  $E_{\text{in}}^{\text{cm}}$  is the incident energy of B in the cm system, i.e.,  $E_{\text{in}}^{\text{cm}} \equiv \hbar^2 \hat{P}_0^2 / (2\mu)$ .

Multiplying Eq. (2.6) by  $\langle \hat{\Phi}_i |$  from the left leads to a set of coupled differential equations for  $|\hat{\chi}_i\rangle$ , called the CDCC equation,

$$[T_R + \hat{U}_{i,i} - E_i]|\hat{\chi}_i\rangle = - \sum_{i' \neq i} \hat{U}_{i,i'} |\hat{\chi}_{i'}\rangle, \quad (2.9)$$

where  $E_i \equiv \hbar^2 \hat{P}_i^2 / (2\mu) = E_{\text{tot}} - \hat{\varepsilon}_i$ . The coupling potential  $\hat{U}_{i,i'}$  is defined by

$$\hat{U}_{i,i'} = \langle \hat{\Phi}_i | U | \hat{\Phi}_{i'} \rangle. \quad (2.10)$$

The CDCC equation (2.9) is solved under the usual boundary condition for  $\langle \mathbf{R} | \hat{\chi}_i \rangle \equiv \hat{\chi}_i(\mathbf{R})$ .<sup>21),22)</sup>

## 2.2. Pseudostate Discretization Method

In the pseudostate discretization method,<sup>27),28),30)–32)</sup> the pseudostates  $\{\hat{\Phi}_i\}$  are obtained by diagonalizing the internal Hamiltonian  $H_B$  of B in a space spanned

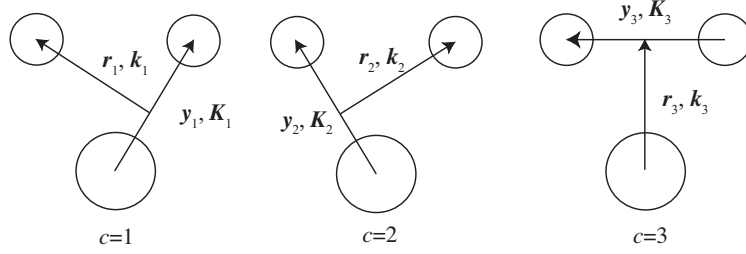


Fig. 2. Jacobi coordinates of the three rearrangement channels ( $c=1-3$ ) in the three-body system. Vectors  $(\mathbf{k}_c, \mathbf{K}_c)$  denote linear momenta conjugate to the coordinates  $(\mathbf{r}_c, \mathbf{y}_c)$ .

by  $L^2$ -type Gaussian basis functions.<sup>34)</sup> The eigenstates of  $H_B$  with negative and positive energies correspond to the bound state(s) and pseudostates, respectively, and the latter are regarded as discretized continuum states as mentioned above. Now we consider  ${}^6\text{He}$  as a projectile. The eigenstate  $\hat{\Phi}_i \equiv \hat{\Phi}_{nIm}$  is then written as

$$\langle \mathbf{r}, \mathbf{y} | \hat{\Phi}_{nIm} \rangle = \sum_{c=1}^3 \psi_{nIm}^{(c)}(\mathbf{r}_c, \mathbf{y}_c), \quad (2-11)$$

where  $c$  denotes a set of Jacobi coordinates defined in Fig. 2. Each  $\psi_{nIm}^{(c)}$  is a sum of the Gaussian basis functions:

$$\begin{aligned} \psi_{nIm}^{(c)}(\mathbf{r}_c, \mathbf{y}_c) &= \sum_{\alpha} A_{\alpha}^{(c)nI} \varphi_{\alpha}^{(c)}(\mathbf{r}_c, \mathbf{y}_c), \quad (2-12) \\ \varphi_{\alpha}^{(c)}(\mathbf{r}_c, \mathbf{y}_c) &= \mathcal{N}_{i\ell} \mathcal{N}_{j\lambda} r_c^{\ell} e^{-\nu_i r_c^2} y_c^{\lambda} e^{-\lambda_j y_c^2} \\ &\quad \times \left[ [Y_{\ell}(\Omega_{r_c}) \otimes Y_{\lambda}(\Omega_{y_c})]_A \otimes [\eta_{1/2}^{(n_1)} \otimes \eta_{1/2}^{(n_2)}]_S \right]_{Im}, \quad (2-13) \end{aligned}$$

where  $\alpha$  is the abbreviation of  $\{i, j, \ell, \lambda, A, S\}$ ;  $\ell$  ( $\lambda$ ) is the orbital angular momentum associated with the coordinate  $\mathbf{r}_c$  ( $\mathbf{y}_c$ ) and  $\eta_{1/2}$  is the spin wave function of each valence neutron,  $n_1$  or  $n_2$ . The normalization coefficients  $\mathcal{N}_{i\ell}$  and  $\mathcal{N}_{j\lambda}$  are determined so as to satisfy  $\langle \mathcal{N}_{i\ell} r_c^{\ell} e^{-\nu_i r_c^2} | \mathcal{N}_{i\ell} r_c^{\ell} e^{-\nu_i r_c^2} \rangle = 1$  and  $\langle \mathcal{N}_{j\lambda} y_c^{\lambda} e^{-\lambda_j y_c^2} | \mathcal{N}_{j\lambda} y_c^{\lambda} e^{-\lambda_j y_c^2} \rangle = 1$ . The quantum numbers  $\ell$ ,  $\lambda$ , and  $A$  are truncated by the upper limit values  $\ell_{\max}$ ,  $\lambda_{\max}$ , and  $A_{\max}$ , respectively. The total spin  $S$  is either 0 or 1. The Gaussian range parameters are given geometric progression:

$$\nu_i = 1/r_i^2, \quad r_i = r_1 (r_{\max}/r_1)^{(i-1)/(i_{\max}-1)}, \quad (2-14)$$

$$\lambda_j = 1/y_j^2, \quad y_j = y_1 (y_{\max}/y_1)^{(j-1)/(j_{\max}-1)}. \quad (2-15)$$

The states  $\hat{\Phi}_{nIm}$  are antisymmetric under the interchange between  $n_1$  and  $n_2$ , and hence they must satisfy  $A_{\alpha}^{(2)nI} = (-)^S A_{\alpha}^{(1)nI}$  and for  $c=3$   $(-)^{\lambda+S} = 1$ . Meanwhile, the exchange between each valence neutron and each nucleon in  ${}^4\text{He}$  is treated approximately by the orthogonality condition model.<sup>35)</sup> The eigenenergies  $\hat{\varepsilon}_{nI}$  of  ${}^6\text{He}$  and the corresponding expansion coefficients  $A_{\alpha}^{(c)nI}$  are determined by diagonalizing  $H_B$ .<sup>36),37)</sup> In the diagonalization procedure one needs the coordinate transformation between the rearrangement channels. Details of this transformation are described in Appendix A.

### 2.3. Smoothing Method

The exact breakup  $T$ -matrix elements to the continuum state  $\psi(\mathbf{k}, \mathbf{K})$  of B are given by

$$T^{\text{EX}}(\mathbf{k}, \mathbf{K}, \mathbf{P}) = \langle \psi(\mathbf{k}, \mathbf{K}), P | U | \Psi \rangle, \quad (2.16)$$

with  $|\psi(\mathbf{k}, \mathbf{K}), P\rangle = |\psi(\mathbf{k}, \mathbf{K})\rangle \otimes |P\rangle$ , where  $\mathbf{k}$ ,  $\mathbf{K}$ , and  $\mathbf{P}$  are the momenta in the asymptotic region associated with the coordinates  $\mathbf{r}$ ,  $\mathbf{y}$ , and  $\mathbf{R}$ , respectively;  $|\psi(\mathbf{k}, \mathbf{K})\rangle$  is the exact three-body wave function of B with the energy  $\varepsilon$  satisfying

$$[H_B - \varepsilon]|\psi(\mathbf{k}, \mathbf{K})\rangle = 0, \quad (2.17)$$

and  $|P\rangle$  is the plane wave function satisfying

$$[T_R - (E_{\text{tot}} - \varepsilon)]|P\rangle = 0. \quad (2.18)$$

The exact four-body (a+b+c+A) wave function  $\Psi$  can be replaced with the corresponding CDCC wave function  $\Psi^{\text{CDCC}}$  with good accuracy. Inserting the approximate complete set  $\mathcal{P}$  of Eq. (2.4) between the bra vector and the operator  $U$  on the right-hand side of Eq. (2.16), we can obtain the approximate smooth  $T$ -matrix elements  $T(\mathbf{k}, \mathbf{K}, \mathbf{P})$ :

$$\begin{aligned} T(\mathbf{k}, \mathbf{K}, \mathbf{P}) &= \sum_i \langle \psi(\mathbf{k}, \mathbf{K}) | \hat{\Phi}_i \rangle \langle \hat{\Phi}_i, \hat{P}_i | U | \Psi^{\text{CDCC}} \rangle \\ &\equiv \sum_i \mathcal{F}_i(\mathbf{k}, \mathbf{K}) \hat{T}_i, \end{aligned} \quad (2.19)$$

where  $|\hat{\Phi}_i, \hat{P}_i\rangle = |\hat{\Phi}_i\rangle \otimes |\hat{P}_i\rangle$ ,  $\mathcal{F}_i(\mathbf{k}, \mathbf{K})$  is the smoothing factor defined by

$$\mathcal{F}_i(\mathbf{k}, \mathbf{K}) = \langle \psi(\mathbf{k}, \mathbf{K}) | \hat{\Phi}_i \rangle, \quad (2.20)$$

and  $\hat{T}_i$  is the breakup  $T$ -matrix element of CDCC defined by

$$\hat{T}_i = \langle \hat{\Phi}_i, \hat{P}_i | U | \Psi^{\text{CDCC}} \rangle. \quad (2.21)$$

Since the breakup  $T$ -matrix elements are proportional to the breakup  $S$ -matrix elements, Eq. (2.19) is reduced to

$$S(\mathbf{k}, \mathbf{K}, \mathbf{P}) = \sum_i \mathcal{F}_i(\mathbf{k}, \mathbf{K}) \hat{S}_i. \quad (2.22)$$

The smoothing factor  $\mathcal{F}_i(\mathbf{k}, \mathbf{K})$  is the overlap between the pseudostate  $\hat{\Phi}_i$  and the exact continuum state  $\psi(\mathbf{k}, \mathbf{K})$ . In principle, the exact continuum state is obtained by solving the three-body Schrödinger equation (2.17) under the initial condition that the three particles a, b, and c, are incident particles. In practice, however, it is quite difficult to do so. Therefore, we approximately solve the equation in the model space  $\mathcal{P}$  of Eq. (2.4):

$$\mathcal{P}|\psi\rangle = \mathcal{P}|\psi_0\rangle + \mathcal{P} \frac{1}{\varepsilon - T_r - T_y + i\epsilon} \mathcal{P} V \mathcal{P} |\psi\rangle, \quad (2.23)$$

where  $V = V_{ab} + V_{bc} + V_{ca}$  and  $\psi_0$  describes free propagation of the three incident particles satisfying

$$[T_r + T_y - \varepsilon] |\psi_0\rangle = 0. \quad (2.24)$$

The solution to Eq. (2.23) should converge as the model space is extended. This is tested in §3. Multiplying Eq. (2.23) by  $\langle \hat{\Phi}_i |$  leads to

$$\mathcal{F}_i(\mathbf{k}, \mathbf{K}) = \tilde{\Phi}_i(\mathbf{k}, \mathbf{K}) + \sum_{jk} G_{ij} V_{jk} \mathcal{F}_k(\mathbf{k}, \mathbf{K}), \quad (2.25)$$

where

$$\tilde{\Phi}_i(\mathbf{k}, \mathbf{K}) = \langle \hat{\Phi}_i | \psi_0 \rangle = \langle \psi_0 | \hat{\Phi}_i \rangle, \quad (2.26)$$

$$G_{ij} = \langle \hat{\Phi}_i | \frac{1}{\varepsilon - T_r - T_y + i\epsilon} | \hat{\Phi}_j \rangle, \quad (2.27)$$

$$V_{jk} = \langle \hat{\Phi}_j | V | \hat{\Phi}_k \rangle. \quad (2.28)$$

Since Eq. (2.25) is a set of linear equations for  $\mathcal{F}_i(\mathbf{k}, \mathbf{K})$ , one can easily obtain a solution for  $\mathcal{F}_i(\mathbf{k}, \mathbf{K})$  once  $\tilde{\Phi}_i(\mathbf{k}, \mathbf{K})$ ,  $G_{ij}$ , and  $V_{jk}$  are evaluated. We emphasize here that what we need in the present smoothing method is not the exact three-body continuum wave function  $\psi(\mathbf{k}, \mathbf{K})$  itself but the smoothing factors  $\mathcal{F}_i(\mathbf{k}, \mathbf{K})$ . In other words, as shown in Eq. (2.20), we need only the overlap between  $\psi(\mathbf{k}, \mathbf{K})$  and  $\hat{\Phi}_i$ ; the latter is an accurate three-body wave function in the model space that is significant for the four-body reaction under consideration. Thus, henceforth, we call this procedure based on model space truncation *the model space smoothing method*. The six-fold integral over  $\mathbf{r}$  and  $\mathbf{y}$  in Eq. (2.26) can be made analytically, and the six-fold integral in Eq. (2.27) is reduced to a single integral. These properties markedly simplify numerical calculations. We show in Appendix B the explicit form of  $\tilde{\Phi}_i(\mathbf{k}, \mathbf{K})$ , i.e., the Fourier transform of  $\hat{\Phi}_i$ , and in Appendix C that of  $G_{ij}$ .

We remark that in  $\mathcal{F}_i(\mathbf{k}, \mathbf{K})$ , or equivalently, in Eq. (2.23), the rearrangement channels of the three particles are fully taken into account. On the other hand, in the calculation of scattering processes by four-body CDCC, we neglect four-body rearrangement channels, in which at least one constituent of the projectile is bound in the target nucleus. The contribution of the rearrangement channels is, however, theoretically shown to be negligible in forward angle scattering.<sup>25),26)</sup> Recently, it has also been confirmed numerically by comparing the results of three-body CDCC for deuteron elastic and breakup processes by  $^{12}\text{C}$  at 56 MeV with the exact solution of the Faddeev equation.<sup>38)</sup> Such a comparison for four-body scattering processes will be very interesting.

### §3. Test Calculations

#### 3.1. Breakup Reaction of Two-body Projectile

In this subsection, we consider the  $^{58}\text{Ni}(d, pn)$  reaction at 80 MeV to test the validity of the model space smoothing method. In this reaction, the projectile ( $d$ )

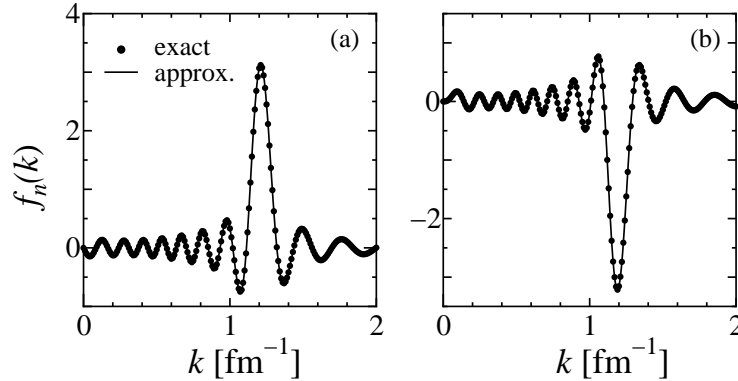


Fig. 3. Smoothing factor as a function of  $k$  for  $n = 16$ . The left (right) panel corresponds to  $\ell = 0$  ( $\ell = 2$ ). The dots and solid curve denote the results of the exact calculation and those obtained by the model space smoothing method, respectively.

consists of a proton ( $p$ ) and a neutron ( $n$ ), and the total system is composed of  $p$ ,  $n$ , and  $A$ . The Coulomb breakup processes are neglected, i.e., Coulomb potential is treated as a function of the relative coordinate  $\mathbf{R}$  between the cm of  $d$  and  $^{58}\text{Ni}$ . We adopt the model space smoothing method described in §2.3 to obtain continuous breakup  $S$ -matrix elements for this reaction. Note that, in this case, the coordinate  $\mathbf{y}$  and its conjugate momentum  $\mathbf{K}$  do not appear and  $\mathbf{r}$  denotes the relative coordinate between  $p$  and  $n$ . As for the interaction between  $p$  and  $n$ , we cite that in Ref. 27). The ground and breakup states of the  $p+n$  subsystem, classified with the linear and angular momenta  $k$  and  $\ell$ , respectively, are obtained by diagonalizing the Hamiltonian of a subsystem with complex-range Gaussian basis functions.<sup>34)</sup> As for the parameter set of the basis functions, we take  $\{2N_{\text{max}} = 40, r_1 = 1.0 \text{ fm}, r_{\text{max}} = 20 \text{ fm}\}$ , where  $2N_{\text{max}}$  is the total number of the basis functions, and  $r_1$  and  $r_{\text{max}}$  are the Gaussian range parameters given in Eq. (2.14). The maximum momentum  $k_{\text{max}}$  is taken to be  $1.3 \text{ fm}^{-1}$ , and the number of states is 17 for each of  $\ell = 0$  and 2. The optical potentials of  $n$ - $^{58}\text{Ni}$  and  $p$ - $^{58}\text{Ni}$  systems are cited from Ref. 27). In solving the CDCC equation, the scattering wave functions are connected with the asymptotic forms at  $R_{\text{max}} = 30 \text{ fm}$ .

When a two-body projectile such as  $d$  is considered, it is possible to obtain an exact smoothing factor without making the model space truncation in Eq. (2.23). In Fig. 3, the approximate smoothing factor with the model space smoothing method (solid curve) is compared with the exact smoothing factor (dots) in the case of  $n = 16$  with  $\ell = 0$  (left panel) and 2 (right panel). In each panel, the two results agree very well with each other. In fact, the difference between the two is below 1% level.

Figure 4 shows the squared magnitudes of the breakup  $S$ -matrix elements for the total angular momentum  $J = 17$ ; panels (a), (b), (c), and (d) correspond to  $(\ell, L) = (0, 17), (2, 15), (2, 17),$  and  $(2, 19)$ , respectively. Again, the results obtained by the model space smoothing method (solid curves) agree very well with the results of the exact calculation (dots).



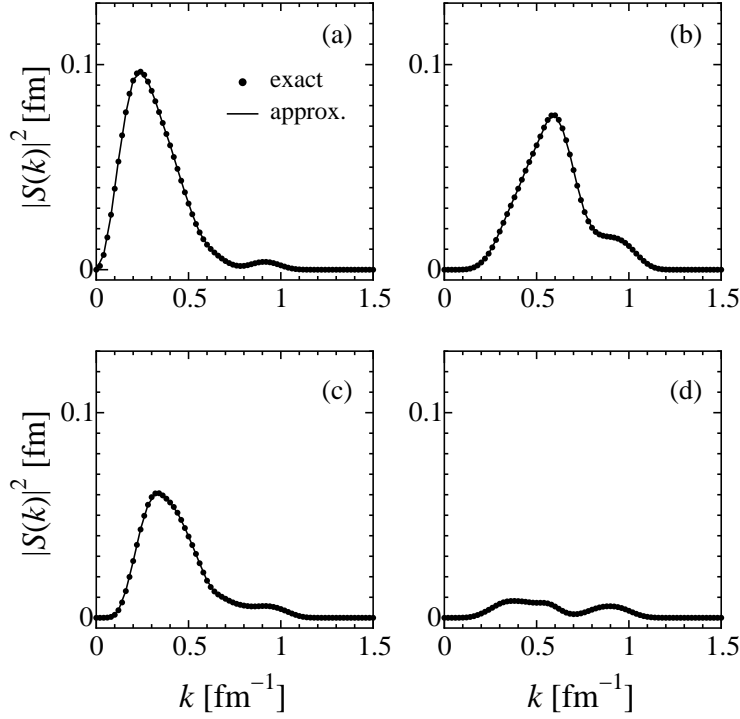


Fig. 4. Squared magnitudes of the smoothed breakup  $S$ -matrix elements  $|S(k)|^2$  as a function of  $k$  at the total angular momentum  $J = 17$  for the  $d+^{58}\text{Ni}$  scattering at 80 MeV. Panels (a), (b), (c), and (d) correspond to  $(\ell, L) = (0, 17)$ ,  $(2, 15)$ ,  $(2, 17)$ , and  $(2, 19)$ , respectively. The results of the exact calculation (model space smoothing method) are shown by the dots (solid curve).

### 3.2. Electric Dipole Transition of $^6\text{He}$ to $1^-$ Continuum States

In the calculation of the  $^4\text{He}+n+n$  three-body wave functions, we take the same Hamiltonian  $H_B$  as that in Ref. 31), which is based on the orthogonality condition model (OCM).<sup>35)</sup> In the present calculation, however, the OCM potential to exclude the forbidden state is introduced into only the  $0^+$  state. Consequently, one can obtain the  $0^+$  ground state of  $^6\text{He}$  while excluding the forbidden state in the diagonalization of  $H_B$ . On the other hand, for the  $1^-$  state, not only the physical pseudostates to be regarded as discretized continuum states of the  $^4\text{He}+n+n$  three-body system, but also unphysical eigenstates that have large overlaps with the forbidden state are obtained, because of the absence of the OCM potential. We exclude the latter by hand, following the variation-before-projection method. This rather special treatment of the  $1^-$  state is due to the following fact. In the present calculation, as one can see below, so many Gaussian basis functions are used for the  $1^-$  state to cover a wide range of internal coordinates concerned. In this case, when an OCM potential that has a core of about  $10^6$  MeV appears, the numerical calculation of the diagonalization of the  $^6\text{He}$  internal Hamiltonian becomes unstable. Note that the  $0^+$  pseudostates and  $2^+$  state of  $^6\text{He}$ , which are included in Ref. 31), are not relevant to the present calculation of the E1 strength distribution of  $^6\text{He}$ .

Table I. Parameters of the basis functions for the  $0^+$  state of  ${}^6\text{He}$ .

$c$	$\ell$	$\lambda$	$A$	$S$	$i_{\max}$	$r_1$ (fm)	$r_{\max}$ (fm)	$j_{\max}$	$y_1$ (fm)	$y_{\max}$ (fm)
3	0	0	0	0	10	0.1	20.0	10	0.5	20.0
1,2	0	0	0	0	10	0.5	20.0	10	0.5	20.0
3	1	1	1	1	10	0.1	20.0	10	0.5	20.0
1,2	1	1	0	0	10	0.5	20.0	10	0.5	20.0
1,2	1	1	1	1	10	0.5	20.0	10	0.5	20.0

Table II. Three parameter sets (I, II, and III) of the basis functions for the  $1^-$  state of  ${}^6\text{He}$ .

Set I

$c$	$\ell$	$\lambda$	$A$	$S$	$i_{\max}$	$r_1$ (fm)	$r_{\max}$ (fm)	$j_{\max}$	$y_1$ (fm)	$y_{\max}$ (fm)
3	0	1	1	0	17	0.5	50.0	17	0.5	50.0
1,2	0	1	1	0	17	0.5	50.0	17	0.5	50.0
1,2	1	0	1	0	17	0.5	50.0	17	0.5	50.0

Set II

3	0	1	1	0	18	0.5	70.0	18	0.5	70.0
1,2	0	1	1	0	18	0.5	70.0	18	0.5	70.0
1,2	1	0	1	0	18	0.5	70.0	18	0.5	70.0

Set III

3	0	1	1	0	19	0.5	80.0	19	0.5	80.0
1,2	0	1	1	0	19	0.5	80.0	19	0.5	80.0
1,2	1	0	1	0	19	0.5	80.0	19	0.5	80.0

As for the basis functions taken in the diagonalization of  $H_B$ , we adopt the real-range Gaussian basis functions. The parameter set for the  $0^+$  state is shown in Table I. For the  $1^-$  state, we take the three parameter sets shown in Table II and see the dependence of the E1 strength distribution on them; the model space described by the  $1^-$  pseudostates of  ${}^6\text{He}$  taken in the calculation dictates the convergence of the E1 distribution. Note that for the  $1^-$  states,  $r_{\max}$  and  $y_{\max}$  are taken to be 50–80 fm to cover the large model space concerned. The  $S = 1$  components of the  $1^-$  states are found to be negligible and not included in the present calculation.

The electric dipole (E1) strength from the  $0^+$  ground state  $\Phi_{00}^{gs}$  to the  $n$ th  $1^-$  pseudostate is

$$B(\text{E1}; n) = N \sum_{\mu m} |\langle \hat{\Phi}_{n1m} | \mathcal{O}_{1\mu}(\text{E1}) | \Phi_{00}^{gs} \rangle|^2, \quad (3.1)$$

where  $\mathcal{O}_{1\mu}(\text{E1}) = r_3 Y_{1\mu}(\Omega_{r_3})$  and  $N = (N_n N_c / A)^2$ . The mass number and neutron number of the core nucleus are denoted  $A$  and  $N_c$ , respectively, and  $N_n$  is the number of valence neutrons; for  ${}^6\text{He}$ ,  $A = 6$  and  $N_n = N_c = 2$ .

Since the final states  $\{\hat{\Phi}_{n1m}\}$  of the E1 transition have discrete energies  $\{\hat{\varepsilon}_n\}$ ,  $B(\text{E1}; n)$  is a discrete function of the energy  $\varepsilon$  of the  ${}^4\text{He}+n+n$  system in the final state, as shown in Fig. 5 (the bars); panels (a), (b), and (c) show the results with Sets I, II, and III, respectively.  $B(\text{E1}; n)$  should be smoothed in some way to be compared with the corresponding experimental data.<sup>9),10)</sup>

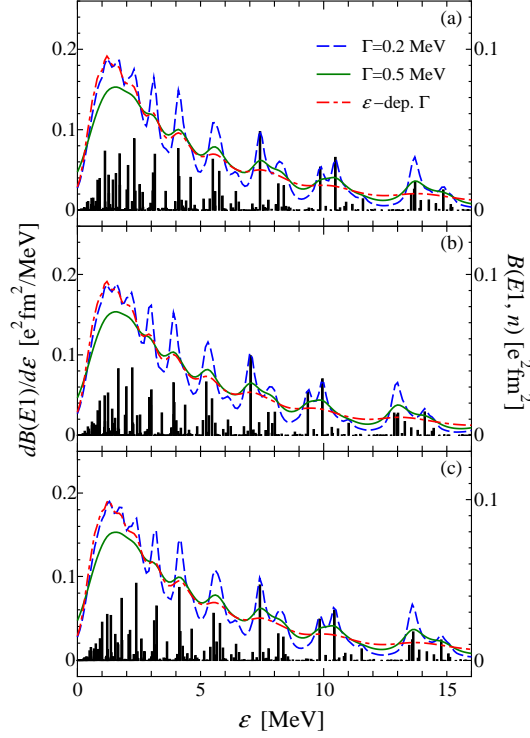


Fig. 5. E1 strength distribution of  ${}^6\text{He}$  as a function of  $\varepsilon$ . In each panel, the bars show  $B(E1; n)$  from the  $0^+$  ground state to the pseudostates of  ${}^6\text{He}$ . Panels (a), (b), and (c) correspond to the results of Sets I, II, and III, respectively. The solid, dashed, and dot-dashed curves respectively show the smeared E1 strength distributions with  $\Gamma = 0.5, 0.2,$  and  $0.1(\hat{\varepsilon}_n + 0.975)$ .

A possible simple way is to assume a Lorentzian function for the  $\varepsilon$  dependence of each  $B(E1; n)$ :<sup>39)</sup>

$$\frac{dB(E1)}{d\varepsilon} = \sum_n \frac{\Gamma}{\pi} \frac{1}{(\varepsilon - \hat{\varepsilon}_n)^2 + \Gamma^2} B(E1; n). \quad (3.2)$$

In Fig. 5, the solid (dashed) curves show the results of Eq. (3.2) with a width  $\Gamma$  of 0.5 (0.2) MeV. With  $\Gamma = 0.2$  MeV, the E1 strength has an unnatural oscillation, which is independent of the parameter set of the basis functions. Even if  $\Gamma$  increases to 0.5 MeV, the distribution becomes smooth only in the small  $\varepsilon$  region of  $\varepsilon \lesssim 3$  MeV. Also shown by the dot-dashed curves are the results with the energy-dependent width  $\Gamma = 0.1(\hat{\varepsilon}_n + 0.975)$  cited from Ref. 9). Again, an unnatural oscillation is found in each panel. In all the cases, unphysically, the smeared distribution is finite at  $\varepsilon = 0$ . Thus, this simple way of smoothing is not helpful for obtaining a result that can be compared with the experimental data.<sup>9), 10)</sup>

The exact E1 strength  $B^{\text{EX}}(E1)$  is defined by

$$B^{\text{EX}}(E1) = N \iint d\mathbf{k} d\mathbf{K} \sum_{\mu m} |\langle \psi_{1m}(\mathbf{k}, \mathbf{K}) | \mathcal{O}_{1\mu}(E1) | \Phi_{00}^{gs} \rangle|^2, \quad (3.3)$$

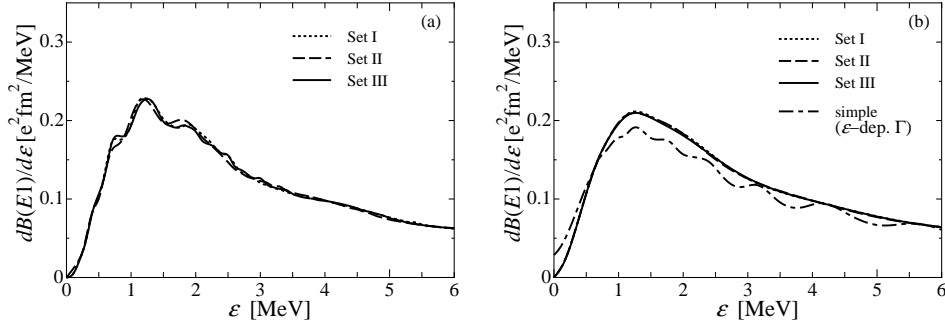


Fig. 6. E1 strength distribution of  ${}^6\text{He}$  as a function of  $\varepsilon$ . The left and right panels correspond to the nonsmeared and smeared results, respectively. In each panel, the dotted, dashed, and solid curves respectively show the results of Sets I, II, and III. Also shown for comparison by the dot-dashed curve is the result of the simple smoothing method with the energy-dependent  $\Gamma$ , i.e., the dot-dashed curve in Fig. 5(c).

where  $\psi_{1m}(\mathbf{k}, \mathbf{K})$  is the exact continuum state of  $1^-$  with the momenta  $\mathbf{k}$  and  $\mathbf{K}$ . The E1 strength distribution function  $dB^{\text{EX}}(E1)/d\varepsilon$  is obtained using

$$\frac{dB^{\text{EX}}(E1)}{d\varepsilon} = N \iint d\mathbf{k}d\mathbf{K} \delta\left(\varepsilon - \frac{\hbar^2 k^2}{2\mu_r} - \frac{\hbar^2 K^2}{2\mu_y}\right) \sum_{\mu m} |\langle \psi_{1m}(\mathbf{k}, \mathbf{K}) | \mathcal{O}_{1\mu}(E1) | \Phi_{00}^{gs} \rangle|^2. \quad (3.4)$$

Inserting the approximate complete set  $\mathcal{P}$  of Eq. (2.4) between the bra vector  $\langle \psi_{1m}(\mathbf{k}, \mathbf{K}) |$  and the operator  $\mathcal{O}_{1\mu}(E1)$  on the right hand side of Eq. (3.4) leads to the E1 strength distribution  $dB(E1)/d\varepsilon$  based on the model space smoothing method:

$$\frac{dB(E1)}{d\varepsilon} = N \iint d\mathbf{k}d\mathbf{K} \delta\left(\varepsilon - \frac{\hbar^2 k^2}{2\mu_r} - \frac{\hbar^2 K^2}{2\mu_y}\right) \sum_{\mu m} \left| \sum_n \mathcal{F}_{n1m}(\mathbf{k}, \mathbf{K}) \mathcal{M}(E1; n) \right|^2, \quad (3.5)$$

where

$$\mathcal{M}(E1; n) = \langle \hat{\Phi}_{n1m} | \mathcal{O}_{1\mu}(E1) | \Phi_{00}^{gs} \rangle, \quad (3.6)$$

$$\mathcal{F}_{n1m}(\mathbf{k}, \mathbf{K}) = \langle \psi_{1m}(\mathbf{k}, \mathbf{K}) | \hat{\Phi}_{n1m} \rangle. \quad (3.7)$$

Thus, the E1 strength distribution function  $dB(E1)/d\varepsilon$  is obtained from the smoothing factor  $\mathcal{F}_{n1m}(\mathbf{k}, \mathbf{K})$  and the discrete E1 transition matrix element  $\mathcal{M}(E1; n)$ . Note that  $\mathcal{M}(E1; n)$  is related to the discrete E1 strength  $B(E1; n)$  through Eq. (3.1). The main task to obtain  $dB(E1)/d\varepsilon$  is, therefore, to evaluate the smoothing factor  $\mathcal{F}_{n1m}(\mathbf{k}, \mathbf{K})$ .

Figure 6(a) shows the dependence of  $dB(E1)/d\varepsilon$  on the model space, i.e., the three parameter sets in Table II. The dotted, dashed, and solid curves represent the results calculated with Sets I, II, and III, respectively. The E1 strength distribution function almost converges as the model space is extended. Strictly speaking, however, the convergence is not perfect. This is because the largest model space of the  ${}^6\text{He}$

wave function that we can treat in the present calculation, i.e., Set III, is still not sufficient to give a perfect convergence. Note that we here consider the Coulomb dipole excitation of  ${}^6\text{He}$ . Since the corresponding interaction has a long range, the model space of  ${}^6\text{He}$ , in the  $1^-$  state in particular, requires quite large values of  $r_{\max}$  and  $y_{\max}$  of the Gaussian basis functions, which considerably increases the number of the basis functions. On the other hand, in the nuclear breakup process of two-body deuteron shown in §3.1, one can prepare an approximate complete set of deuteron quite easily, because not only this breakup potential concerned is short-ranged but also deuteron has only one internal coordinate.

Thus, at this stage the model space smoothing method cannot give a pure theoretical result fully converged owing to computational limits. In order to compare the theoretical result with experimental data, however, one may use an additional smearing procedure that takes account of experimental resolution. This procedure is expressed by

$$\left\langle \frac{dB(\text{E1})}{d\varepsilon} \right\rangle = \int d\varepsilon' w(\varepsilon, \varepsilon') \frac{dB(\text{E1})}{d\varepsilon'}. \quad (3.8)$$

As for the weight function  $w(\varepsilon, \varepsilon')$ , we use the Lorentzian distribution with an energy-dependent width  $\Gamma = 0.1(\varepsilon' + 0.975)$  cited from Ref. 9). Figure 6(b) represents the model space dependence of the E1 strength distribution function smeared with Eq. (3.8). A clear convergence is seen in the figure and the result converged is consistent with those of the other existing methods.<sup>40)–43)</sup> This is also the case if we adopt the Gaussian distribution for  $w(\varepsilon, \varepsilon')$ ; the difference in the result from that with the Lorentzian distribution is within the thickness of the curve shown in Fig. 6(b), at least for  $\varepsilon \lesssim 10$  MeV. Also, as shown in Fig. 6(b), the dot-dashed curve represents the result of the simple smoothing method of Eq. (3.2) with Set III and the energy-dependent  $\Gamma$ , i.e., the dot-dashed curve in Fig. 5(c). One sees the dot-dashed curve deviates considerably from the solid curve. Thus, the simple smoothing method is not accurate as mentioned above. This is found to be also the case when the above-mentioned  $w(\varepsilon, \varepsilon')$  is taken in the simple smoothing method using Eq. (3.2).

Through the tests in §3.1 and 3.2, one can say that the model space smoothing method is reliable in the description of experimental data of the breakup reactions concerned. Therefore, four-body CDCC based on the pseudostate discretization method and the model space smoothing method is expected to be applicable to four-body Coulomb and nuclear breakup reactions such as the ( ${}^6\text{He}, {}^4\text{He}nn$ ) reaction.

#### §4. Application to Four-Body Breakup Cross Section

In this section, we apply the model space smoothing method to the breakup reaction of  ${}^6\text{He}$  by  ${}^{209}\text{Bi}$  at 22.5 MeV. The four-body Hamiltonian  $H$  taken here is the same as that in Ref. 32) except that the OCM potential is introduced into only the  $0^+$  state of  ${}^6\text{He}$ . Moreover, since this is the first trial of four-body CDCC to *real* four-body breakup reactions, for simplicity, the model space in the present four-body CDCC calculation is taken to be smaller than that in Ref. 32); we include only

the  $0^+$  ground state and  $1^-$  pseudostates of  ${}^6\text{He}$  in the coupled-channel calculation. These states are obtained as in §3.2; the parameter set I is used for the  $1^-$  state. In CDCC calculation, the maximum internal energy  $\varepsilon_{\text{max}}$  of  ${}^6\text{He}$  is taken to be 7 MeV, which results in 170  $1^-$  pseudostates. The scattering waves between  ${}^6\text{He}$  and  ${}^{209}\text{Bi}$  are numerically integrated up to  $R_{\text{max}} = 200$  and connected with the asymptotic forms. The maximum total angular momentum  $J_{\text{max}}$  is taken to be 200.

The angle-integrated breakup cross section to the continuous breakup channel with the momenta  $\mathbf{k}$  and  $\mathbf{K}$  is given by

$$\sigma(\mathbf{k}, \mathbf{K}) = \sum_{J,L} \frac{\pi(2J+1)}{P_0^2} \left| \sum_{Im} S_{IL}^J(\mathbf{k}, \mathbf{K}) \right|^2, \quad (4.1)$$

where  $P_0$  is the initial momentum of  ${}^6\text{He}$  in the cm system,  $J$  is the total angular momentum of the four-body system, and  $S_{IL}^J(\mathbf{k}, \mathbf{K})$  is the breakup  $S$ -matrix element for the transition from the initial channel to the breakup channel with  $(I, L, J)$ . Here,  $I$  is the total spin of the projectile, and  $L$  is the orbital angular momentum associated with  $\mathbf{R}$ .

Inserting the partial-wave expansion form of Eq. (2.22) into Eq. (4.1), one can find

$$\sigma(\mathbf{k}, \mathbf{K}) = \sum_{J,L} \frac{\pi(2J+1)}{P_0^2} \left| \sum_{nIm} \mathcal{F}_{nIm}(\mathbf{k}, \mathbf{K}) \hat{S}_{nIL}^J \right|^2, \quad (4.2)$$

where  $\hat{S}_{nIL}^J$  is the discrete breakup  $S$ -matrix element for the transition from the initial channel to the  $n$ th discrete breakup channel with the quantum numbers  $(I, L, J)$ . Thus, the angle-integrated energy spectrum of the breakup reaction is obtained by

$$\frac{d\sigma}{d\varepsilon} = \iint d\mathbf{k} d\mathbf{K} \delta\left(\varepsilon - \frac{\hbar^2 k^2}{2\mu_r} - \frac{\hbar^2 K^2}{2\mu_y}\right) \sigma(\mathbf{k}, \mathbf{K}). \quad (4.3)$$

Since we do not obtain a fully converged theoretical result, we calculate, as in §3.2, the smeared result with

$$\left\langle \frac{d\sigma}{d\varepsilon} \right\rangle = \int d\varepsilon' w(\varepsilon, \varepsilon') \frac{d\sigma}{d\varepsilon}, \quad (4.4)$$

$$w(\varepsilon, \varepsilon') = \frac{0.1(\varepsilon' + 0.975)}{\pi} \frac{1}{(\varepsilon - \varepsilon')^2 + \{0.1(\varepsilon' + 0.975)\}^2}. \quad (4.5)$$

Figure 7 shows the result of  $\langle d\sigma/d\varepsilon \rangle$  as a function of  $\varepsilon$ . The solid curve is the result of four-body CDCC and the dashed curve is the result of the one-step calculation in which only one-step transition from the elastic channel to the individual breakup channels is taken into account. The latter is significantly larger than the former. This clearly shows the significant reduction in the size of the breakup cross section due to multistep transition. Furthermore, the two calculations give quite different  $\varepsilon$  dependences for  $\varepsilon \gtrsim 2$  MeV. Therefore, the assumption of a one-step transition is not valid at low incident energies. The one-step assumption is often adopted when E1 strength distribution is derived from a measured breakup cross section. Even

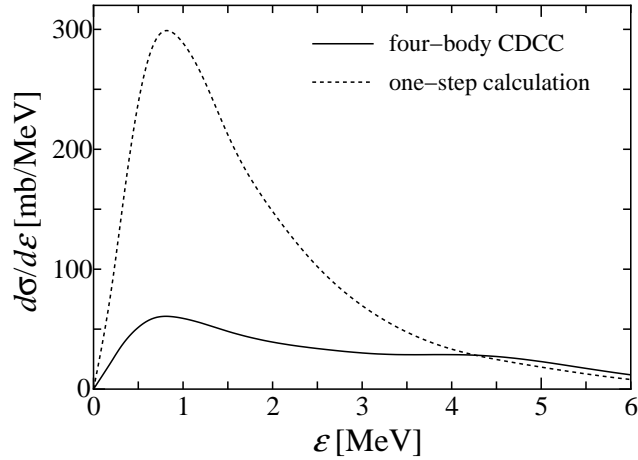


Fig. 7. Angle-integrated energy spectrum  $\langle d\sigma/d\varepsilon \rangle$  of  ${}^6\text{He}+{}^{209}\text{Bi}$  scattering at 22.5 MeV. The solid curve shows the result of the four-body CDCC calculation and the dotted curve shows the result of the one-step calculation. These results have been smeared by the same procedure described in §3.2.

though this has been conducted at higher incident energies,<sup>9),10)</sup> where multistep processes are expected to be less important, it will be very interesting and important to quantitatively evaluate the contributions of multistep breakup processes in this energy region.

## §5. Summary

We propose a new smoothing method based on model space truncation, i.e., *the model space smoothing method*, for constructing a smooth breakup cross section from a discrete one obtained CDCC. This method allows the evaluation of not only three-body breakup cross sections but also four-body ones, which is an important advantage to the smoothing method established so far.

The reliability of the model space smoothing method is confirmed in the two cases:  ${}^{58}\text{Ni}(d, pn)$  at 80 MeV and the E1 transition of  ${}^6\text{He}$ . In the former, the new model space smoothing method is found to give the same breakup  $S$ -matrix elements as the “exact” ones based on the previous smoothing method in Ref. 27). In the latter, the E1 strength distribution obtained by the model space smoothing method, with the additional smearing procedure of Eq. (3·8), turns out to converge well as the model space is extended.

We apply the model space smoothing method to the  ${}^6\text{He}$  scattering on  ${}^{209}\text{Bi}$  at 22.5 MeV, i.e., near the Coulomb barrier energy, and calculate the angle-integrated energy spectrum of the four-body breakup reaction. Comparing the result of the four-body CDCC calculation with that of the one-step calculation, we find that the one-step calculation is not accurate at low incident energies.

Thus, the description of four-body breakup reactions with four-body CDCC is accomplished by the model space smoothing method proposed in this work. In a

forthcoming paper, we will analyze the experimental data on the angle-integrated energy spectrum  $d\sigma/d\varepsilon$ <sup>(9), (10)</sup> and the energy and angular correlations<sup>(8)</sup> among  ${}^4\text{He}$  and the two neutrons in the breakup of  ${}^6\text{He}$  at lower and intermediate incident energies.

### Acknowledgements

The authors would like to thank Prof. M. Kamimura and Prof. Y. Iseri for helpful discussions. This work has been supported in part by JSPS Research Fellowships for Young Scientists and Grants-in-Aid for Scientific Research of Monbukagakusyo of Japan. One of the authors (T. M.) is grateful for the financial assistance from the Special Postdoctoral Researchers Program of RIKEN. The numerical calculations of this work were performed on the computing system in Research Institute for Information Technology of Kyushu University.

### Appendix A

#### — Coordinate Transformation Between Rearrangement Channels —

The coordinate transformation from  $(\mathbf{r}_b, \mathbf{y}_b)$  to  $(\mathbf{r}_c, \mathbf{y}_c)$  is defined by

$$\begin{pmatrix} \mathbf{r}_b \\ \mathbf{y}_b \end{pmatrix} = \begin{pmatrix} \gamma_{bc} & \delta_{bc} \\ \gamma'_{bc} & \delta'_{bc} \end{pmatrix} \begin{pmatrix} \mathbf{r}_c \\ \mathbf{y}_c \end{pmatrix}. \quad (\text{A}\cdot 1)$$

With this transformation, the basis function  $\varphi_{\alpha_b}^{(b)}(\mathbf{r}_b, \mathbf{y}_b)$  is rewritten as

$$\begin{aligned} & \varphi_{\alpha_b}^{(b)}(\mathbf{r}_c, \mathbf{y}_c) \\ &= \mathcal{N}_{i_b \ell_b} \mathcal{N}_{j_b \lambda_b} e^{-\eta_{bc} r_c^2} e^{-2\xi_{bc} \mathbf{r}_c \cdot \mathbf{y}_c} e^{-\zeta_{bc} y_c^2} \sum_{\ell'_b, \lambda'_b, T} \langle \ell_b \lambda_b A_b | \ell'_b \lambda'_b T A_b \rangle_{b \rightarrow c} \\ & \quad \times r_c^{\ell_b + \lambda_b - T} y_c^T \left[ [Y_{\ell'_b}(\Omega_{r_c}) \otimes Y_{\lambda'_b}(\Omega_{y_c})]_{A_b} \otimes [\eta_{1/2}^{(n_1)} \otimes \eta_{1/2}^{(n_2)}]_{S_b} \right]_{I_m}, \end{aligned} \quad (\text{A}\cdot 2)$$

where  $\alpha_b$  is the abbreviation of  $\{i_b, j_b, \ell_b, \lambda_b, A_b, S_b\}$  for channel  $b$  and

$$\eta_{bc} = \nu_{i_b} \gamma_{bc}^2 + \lambda_{j_b} \gamma'_{bc}{}^2, \quad (\text{A}\cdot 3)$$

$$\zeta_{bc} = \nu_{i_b} \delta_{bc}^2 + \lambda_{j_b} \delta'_{bc}{}^2, \quad (\text{A}\cdot 4)$$

$$\xi_{bc} = \nu_{i_b} \delta_{bc} \gamma_{bc} + \lambda_{j_b} \delta'_{bc} \gamma'_{bc}. \quad (\text{A}\cdot 5)$$

The coefficient  $\langle \ell_b \lambda_b A_b | \ell'_b \lambda'_b T A_b \rangle_{b \rightarrow c}$  in Eq. (A·2) is that of the Raynal transformation defined by

$$\begin{aligned} & \sum_{\ell'_b, \lambda'_b, T} \langle \ell_b \lambda_b A_b | \ell'_b \lambda'_b T A_b \rangle_{b \rightarrow c} r_c^{\ell_b + \lambda_b - T} y_c^T [Y_{\ell'_b}(\Omega_{r_c}) \otimes Y_{\lambda'_b}(\Omega_{y_c})]_{A_b} \\ &= (2\ell_b + 1)(2\lambda_b + 1) \sum_{\lambda=0}^{\ell_b} \sum_{A=0}^{\lambda_b} \sqrt{\frac{(2\ell_b)!}{(2\lambda)!(2\ell_b - 2\lambda)!}} \sqrt{\frac{(2\lambda_b)!}{(2A)!(2\lambda_b - 2A)!}} \end{aligned}$$



$$\begin{aligned}
 & \times \gamma_{bc}^{\ell_b - \lambda} \gamma'_{bc}{}^{\lambda_b - \Lambda} \delta_{bc}^\lambda \delta'_{bc}{}^\Lambda \sum_{\ell'_b \lambda'_b} \left\{ \begin{array}{ccc} \ell_b - \lambda & \lambda_b - \Lambda & \ell'_b \\ \lambda & \Lambda & \lambda'_b \\ \ell_b & \lambda_b & \Lambda_b \end{array} \right\} \langle \ell_b - \lambda 0 \lambda_b - \Lambda 0 | \ell'_b 0 \rangle \langle \lambda 0 \Lambda 0 | \lambda'_b 0 \rangle \\
 & \times r_c^{\ell_b + \lambda_b - \lambda + \Lambda} y_c^{\lambda + \Lambda} [Y_{\ell'_b}(\Omega_{r_c}) \otimes Y_{\lambda'_b}(\Omega_{y_c})]_{A_b}, \tag{A.6}
 \end{aligned}$$

where  $T = \lambda + \Lambda$ .

## Appendix B

### — Fourier Transform of $\hat{\Phi}_{nIm}(\mathbf{r}, \mathbf{y})$ —

The Fourier transform  $\tilde{\Phi}_{nIm}(\mathbf{k}, \mathbf{K})$  of  $\hat{\Phi}_{nIm}(\mathbf{r}, \mathbf{y})$  has the form

$$\begin{aligned}
 \tilde{\Phi}_{nIm}(\mathbf{k}, \mathbf{K}) &= \frac{1}{(2\pi)^3} \iint d\mathbf{r} d\mathbf{y} e^{i\mathbf{k}\cdot\mathbf{r}} e^{i\mathbf{K}\cdot\mathbf{y}} \hat{\Phi}_{nIm}(\mathbf{r}, \mathbf{y}) \\
 &= \frac{1}{(2\pi)^3} \sum_{c,\alpha} A_\alpha^{(c)nI} \tilde{\varphi}_\alpha^{(c)}(\mathbf{k}_c, \mathbf{K}_c) \tag{B.1}
 \end{aligned}$$

with

$$\begin{aligned}
 \tilde{\varphi}_{\alpha_c}^{(c)}(\mathbf{k}_c, \mathbf{K}_c) &= \mathcal{N}_{i_c \ell_c} \mathcal{N}_{j_c \lambda_c} \left( \frac{\pi}{\nu_{i_c}} \right)^{3/2} \left( \frac{\pi}{\lambda_{j_c}} \right)^{3/2} \left( \frac{i}{2\nu_{i_c}} \right)^{\ell_c} \left( \frac{i}{2\lambda_{j_c}} \right)^{\lambda_c} \\
 & \times k_c^{\ell_c} e^{-k_c^2/4\nu_{i_c}} K_c^{\lambda_c} e^{-K_c^2/4\lambda_{j_c}} \left[ [Y_{\ell_c}(\Omega_{k_c}) \otimes Y_{\lambda_c}(\Omega_{K_c})]_{A_c} \otimes [\eta_{1/2}^{(n_1)} \otimes \eta_{1/2}^{(n_2)}]_{S_c} \right]_{Im}. \tag{B.2}
 \end{aligned}$$

Performing the coordinate transformation of Eq. (A.1) leads to

$$\begin{aligned}
 & \tilde{\varphi}_{\alpha_b}^{(b)}(\mathbf{k}_c, \mathbf{K}_c) \\
 &= \mathcal{N}_{i_b \ell_b} \mathcal{N}_{j_b \lambda_b} \left( \frac{\pi}{\nu_{i_b}} \right)^{3/2} \left( \frac{\pi}{\lambda_{j_b}} \right)^{3/2} \left( \frac{i}{2\nu_{i_b}} \right)^{\ell_b} \left( \frac{i}{2\lambda_{j_b}} \right)^{\lambda_b} \\
 & \times e^{-\eta'_{bc} k_c^2} e^{-2\xi'_{bc} \mathbf{k}_c \cdot \mathbf{K}_c} e^{-\zeta'_{bc} K_c^2} \sum_{\ell'_b, \lambda'_b, T} \langle \ell_b \lambda_b A_b | \ell'_b \lambda'_b T A_b \rangle_{b \rightarrow c} \\
 & \times k_c^{\ell_b + \lambda_b - T} K_c^T \left[ [Y_{\ell'_b}(\Omega_{k_c}) \otimes Y_{\lambda'_b}(\Omega_{K_c})]_{A_b} \otimes [\eta_{1/2}^{(n_1)} \otimes \eta_{1/2}^{(n_2)}]_{S_b} \right]_{Im} \tag{B.3}
 \end{aligned}$$

with

$$\eta'_{bc} = \frac{1}{4\nu_{i_b}} \bar{\gamma}_{bc}^2 + \frac{1}{4\lambda_{j_b}} \bar{\gamma}'_{bc}{}^2, \tag{B.4}$$

$$\zeta'_{bc} = \frac{1}{4\nu_{i_b}} \bar{\delta}_{bc}^2 + \frac{1}{4\lambda_{j_b}} \bar{\delta}'_{bc}{}^2, \tag{B.5}$$

$$\xi'_{bc} = \frac{1}{4\nu_{i_b}} \bar{\delta}_{bc} \bar{\gamma}_{bc} + \frac{1}{4\lambda_{j_b}} \bar{\delta}'_{bc} \bar{\gamma}'_{bc}, \tag{B.6}$$

where

$$\bar{\gamma}_{bc} = \gamma_{cb}, \quad \bar{\delta}_{bc} = \gamma'_{cb}, \quad \bar{\gamma}'_{bc} = \delta_{cb}, \quad \bar{\delta}'_{bc} = \delta'_{cb}. \tag{B.7}$$

### Appendix C

— Matrix Elements of  $G_{ij}$  —

In  $G_{ij}$  the six-fold integration is reduced to a single one:

$$G_{ij} = \sum_{a=1}^3 \sum_{b=1}^3 \sum_{\alpha_a} \sum_{\alpha_b} A_{\alpha_a}^{(a)iI} A_{\alpha_b}^{(b)jI} \tilde{G}_{\alpha_a \alpha_b}, \quad (\text{C}\cdot 1)$$

where  $\alpha_c = \{i_c, j_c, \ell_c, \lambda_c, \Lambda_c, S_c\}$  for channel  $c$  ( $=1-3$ ) and  $\tilde{G}_{\alpha_a \alpha_b}$  is given by

$$\begin{aligned} & \tilde{G}_{\alpha_a \alpha_b} \\ &= \delta_{\Lambda_a \Lambda_b} \delta_{SS'} \frac{(-)^{\Lambda_b}}{(2\pi)^6} \left( \frac{\pi}{\nu_{i_a}} \frac{\pi}{\lambda_{j_a}} \frac{\pi}{\nu_{i_b}} \frac{\pi}{\lambda_{j_b}} \right)^{3/2} \left( \frac{-i}{2\nu_{i_a}} \right)^{\ell_a} \left( \frac{-i}{2\lambda_{j_a}} \right)^{\lambda_a} \left( \frac{i}{2\nu_{i_b}} \right)^{\ell_b} \left( \frac{i}{2\lambda_{j_b}} \right)^{\lambda_b} \\ & \times \sum_{\ell'_a \lambda'_a T} \langle \ell_a \lambda_a \Lambda_a | \ell'_a \lambda'_a T \Lambda_a \rangle_{a \rightarrow b} \hat{\ell}'_a \hat{\lambda}'_a \hat{\ell}_b \hat{\lambda}_b \sum_{\kappa} W(\lambda'_a, \lambda_b, \ell'_a, \ell_b; \kappa \Lambda_b) \\ & \times \langle \ell'_a 0 \ell_b 0 | \kappa 0 \rangle \langle \lambda'_a 0 \lambda_b 0 | \kappa 0 \rangle \frac{\pi(2m+2\kappa+1)!!}{2^{m+\kappa+n+4}} \sum_{k=0}^m \frac{(2k+2\kappa+2n+1)!!}{(2k+2\kappa+1)!!} \binom{m}{k} \\ & \times (-i) \int_0^\infty d\tau e^{i\tau\varepsilon} \frac{(\eta' + i\tau\tilde{\mu}_r)^{n-m} (\xi')^{2k+\kappa}}{((\zeta' + i\tau\tilde{\mu}_y)(\eta' + i\tau\tilde{\mu}_r) - (\xi')^2)^{k+\kappa+n+3/2}} \end{aligned} \quad (\text{C}\cdot 2)$$

with

$$\begin{aligned} \tilde{\mu}_r &= \hbar^2 k_b^2 / (2\mu_{r_b}), & \tilde{\mu}_y &= \hbar^2 K_b^2 / (2\mu_{y_b}), \\ \eta' &= \eta'_{ab} + 1/(4\nu_{i_b}), & \zeta' &= \zeta'_{ab} + 1/(4\lambda_{j_b}), & \xi' &= \xi'_{ab}, \\ 2n &= \ell_a + \ell_b + \lambda_a - T - \kappa, & 2m &= \lambda_b + T - \kappa, \end{aligned}$$

and  $\hat{\ell} = \sqrt{2\ell+1}$  and  $W(a, b, c, d; e, f)$  is the Racah coefficient. The use of Eqs. (B·3) and (C·2) greatly simplifies numerical calculations.

### References

- 1) I. Tanihata, D. Hirata, T. Kobayashi, S. Shimoura, K. Sugimoto and H. Toki, Phys. Lett. B **289** (1992), 261.
- 2) I. Tanihata, J. of Phys. G **22** (1996), 157.
- 3) P. G. Hansen, A. S. Jensen and B. Jonson, Annu. Rev. Nucl. Part. Sci. **45** (1995), 591.
- 4) E. F. Aguilera *et al.*, Phys. Rev. Lett. **84** (2000), 5058.
- 5) E. F. Aguilera *et al.*, Phys. Rev. C **63** (2001), 061603(R).
- 6) A. M. Sánchez-Beníez *et al.*, Nucl. Phys. A **803** (2008), 30.
- 7) O. R. Kakuee *et al.*, Nucl. Phys. A **728** (2003), 339.
- 8) L. V. Chulkov *et al.*, Nucl. Phys. A **759** (2005), 23.
- 9) T. Aumann *et al.*, Phys. Rev. C **59** (1999), 1252.
- 10) J. Wang *et al.*, Phys. Rev. C **65** (2002), 034306.
- 11) V. Lapoux *et al.*, Phys. Rev. C **66** (2002), 034608.
- 12) M. Milin *et al.*, Nucl. Phys. A **730** (2004), 285.
- 13) J. S. Al-Khalili, I. J. Thompson and J. A. Tostevin, Nucl. Phys. A **581** (1995), 331.
- 14) J. S. Al-Khalili *et al.*, Phys. Lett. B **378** (1996), 45.
- 15) J. A. Christley, J. S. Al-Khalili, J. A. Tostevin and R. C. Johnson, Nucl. Phys. A **624** (1997), 275.

- 16) R. C. Johnson, J. S. Al-Khalili and J. A. Tostevin, *Phys. Rev. Lett.* **79** (1997), 2771.
- 17) R. Crespo and R. C. Johnson, *Phys. Rev. C* **60** (1999), 034007.
- 18) R. Chatterjee, P. Banerjee and R. Shyam, *Nucl. Phys. A* **692** (2001), 476.
- 19) S. N. Ershov, B. V. Danilin and J. S. Vaagen, *Phys. Rev. C* **64** (2001), 064609.
- 20) S. N. Ershov, B. V. Danilin and J. S. Vaagen, *Phys. Rev. C* **74** (2006), 014603.
- 21) M. Kamimura, M. Yahiro, Y. Iseri, Y. Sakuragi, H. Kameyama and M. Kawai, *Prog. Theor. Phys. Suppl.* No. 89 (1986), 1 and references therein.
- 22) N. Austern, Y. Iseri, M. Kamimura, M. Kawai, G. Rawitscher and M. Yahiro, *Phys. Rep.* **154** (1987), 125 and references therein.
- 23) M. Yahiro, M. Nakano, Y. Iseri and M. Kamimura, *Prog. Theor. Phys.* **67** (1982), 1467.
- 24) R. A. D. Piyadasa, M. Yahiro, M. Kamimura and M. Kawai, *Prog. Theor. Phys.* **81** (1989), 910.
- 25) N. Austern, M. Yahiro and M. Kawai, *Phys. Rev. Lett.* **63** (1989), 2649.
- 26) N. Austern, M. Kawai and M. Yahiro, *Phys. Rev. C* **53** (1996), 314.
- 27) T. Matsumoto, T. Kamizato, K. Ogata, Y. Iseri, E. Hiyama, M. Kamimura and M. Yahiro, *Phys. Rev. C* **68** (2003), 064607.
- 28) T. Egami, K. Ogata, T. Matsumoto, Y. Iseri, M. Kamimura and M. Yahiro, *Phys. Rev. C* **70** (2004), 047604.
- 29) A. M. Moro, F. Pérez-Bernal, J. M. Arias and J. Gómez-Camacho, *Phys. Rev. C* **73** (2006), 044612.
- 30) T. Matsumoto, E. Hiyama, M. Yahiro, K. Ogata, Y. Iseri and M. Kamimura, *Nucl. Phys. A* **783c** (2004), 471.
- 31) T. Matsumoto, E. Hiyama, K. Ogata, Y. Iseri, M. Kamimura, S. Chiba and M. Yahiro, *Phys. Rev. C* **70** (2004), 061601(R).
- 32) T. Matsumoto, T. Egami, K. Ogata, Y. Iseri, M. Kamimura and M. Yahiro, *Phys. Rev. C* **73** (2006), 051602(R).
- 33) M. Rodríguez-Gallardo, J. M. Arias, J. Gómez-Camacho, R. C. Johnson, A. M. Moro, I. J. Thompson and J. A. Tostevin, *Phys. Rev. C* **77** (2008), 064609.
- 34) E. Hiyama, Y. Kino and M. Kamimura, *Prog. Part. Nucl. Phys.* **51** (2003), 223.
- 35) S. Saito, *Prog. Theor. Phys.* **41** (1969), 705.
- 36) S. Funada, H. Kameyama and Y. Sakuragi, *Nucl. Phys. A* **575** (1994), 93.
- 37) E. Hiyama and M. Kamimura, *Nucl. Phys. A* **588** (1995), 35c.
- 38) A. C. Fonseca, *Nucl. Phys. A* **805** (2008), 180c.  
A. Deltuva, A. M. Moro, E. Cravo, F. M. Nunes and A. C. Fonseca, *Phys. Rev. C* **76** (2007), 064602.
- 39) K. Hagino and H. Sagawa, *Phys. Rev. C* **72** (2005), 044321; we have corrected the left-hand side of Eq. (18),  $B(E1)$ , to  $dB(E1)/d\varepsilon$ .
- 40) A. Cobis, D. V. Fedorov and A. S. Jensen, *Phys. Rev. Lett.* **79** (1997), 2411.
- 41) B. V. Danilin, I. J. Thompson, J. S. Vaagen and M. V. Zhukov, *Nucl. Phys. A* **632** (1998), 383.
- 42) T. Myo, K. Katō, S. Aoyama and K. Ikeda, *Phys. Rev. C* **63** (2001), 054313.
- 43) S. Aoyama, T. Myo, K. Katō and K. Ikeda, *Prog. Theor. Phys.* **116** (2006), 1.